EEET ECOLOGICAL ENGINEERING & ENVIRONMENTAL TECHNOLOGY

Ecological Engineering & Environmental Technology 2022, 23(5), 234–255
https://doi.org/10.12912/27197050/152141
ISSN 2719-7050, License CC-BY 4.0

Received: 2022.07.02
Accepted: 2022.07.20
Published: 2022.08.01

Use of GIS, Remote Sensing and Analytical Hierarchy Process for Groundwater Potential Assessment in an Arid Region – A Case Study

Abdessamad Jari[1*], El Mostafa Bachaoui[1], Amine Jellouli[1], Abderrazak El Harti[1], Achraf Khaddari[2], Aafaf El Jazouli[1]

[1] Laboratory of Geomatic, Georesources and Environment, Faculty of Sciences and Techniques, Sultan Moulay Slimane University, Mghilla Campus, PB 523, 23000 Beni Mellal, Marocco

[2] Laboratory of Geosciences, Faculty of Sciences, Ibn Tofail University, Morocco University Campus, PB 133, Kenitra, Morocco

* Corresponding author's e-mail: jari.geominesfpt@gmail.com

ABSTRACT

This research aims to evaluate the groundwater potentiality in the arid region "Telmzoun" located in the south of Morocco using the analytical hierarchy process (AHP) model of multi-criteria analysis in conjunction with geographic information system (GIS) and remote sensing techniques. The used methodology to generate the groundwater potential map starts with the preparation of thematic layers of different factors influencing the existence of groundwater, such as precipitation, lithology, geomorphology, lineament density, drainage density, slope, in addition to the proximity of the hydrographic network. Groundwater potential map was prepared using relative weights derived from the AHP. The results were mapped on ArcGIS 10.2 and validated using the existing borehole data and the ROC curve. The accuracy of the generated map reached over 70%. It represents five classes of groundwater potential that are as follows: very high potential areas consisting of 10.5% (2.14 km^2), high potential representing a rate of 27.2% (5.53 km^2), moderate potential areas consisting of 30% (6.06 km^2), low potential 20.5% (4.17 km^2) and very low potential areas showing a rate of 11.8% (2.40 km^2) of the total study area. The results obtained are satisfactory and consist of a guide map to be used effectively in direct future groundwater exploration campaigns and to minimize various field costs.

Keywords: geographic information system, remote sensing, analytical hierarchy process, groundwater, anti atlas belt.

INTRODUCTION

Groundwater is an indispensable resource in the socio-economic development of arid regions and the stabilization of their populations. It constitutes the primary source of drinking water supply for its populations as well as the main engine for the evolution of its agricultural activities (Namous et al. 2021). However, access to these waters is often difficult, particularly in arid climate regions with crystalline basements, because they are characterized by a complexity of hydrogeological contexts accompanied by a spatiotemporal limitation of precipitation (Yao et al. 2016). These geo-climatic conditions complicate the operation of choosing suitable sites for water drilling in many regions of the world (Venkateswaran & Ayyandurai 2015; Yao et al. 2016). Hence several boreholes are dry or have very low yield rates.

In order to reduce the failure rate and to fight against the indiscriminate implementation of water catchment boreholes, several techniques and methods have been developed to preliminarily assess the groundwater potential in a given area. Therefore, two

methodological and technical approaches are widely used: (i) conventional techniques based mainly on on-site investigations, such as reconnaissance drilling, stratigraphic analysis, and geophysics which often give suitable results, but are costly and time-consuming (Mogaji & Omobude 2017; Martín-Loeches et al. 2018), (ii) techniques involving modern geospatial tools such as GIS and Remote Sensing, which are currently considered as fast and less costly groundwater potential assessment techniques (Magesh et al. 2012; Rajan Girija & Mayappan 2019; Al-Djazouli et al. 2021), which will also be examined in this study. The principle of the latter techniques is based on the integration of spatial geo-hydrological factors conditioning the occurrence of groundwater in probabilistic and/or empirical models in order to calculate the groundwater potential index, serving as a preliminary assessment of the groundwater potential in a given region in previous studies (Shekhar & Pandey 2015; Ferozur et al. 2019). Remote sensing has been used for the rapid production of geomorphology, slope, lineament and land cover layer in extensive or even inaccessible areas (Venkateswaran & Ayyandurai 2015; Das & Mukhopadhyay 2020). In addition, GIS has offered the advantage of storing and managing voluminous spatial data useful in the management of groundwater resources (Park et al. 2017) and thus integrating them with great flexibility in different types of models (Park et al. 2017; Al-Ruzouq et al. 2019). Recently, several researchers have used different probabilistic models for the evaluation of groundwater potential such as certainty factor (Razandi et al. 2015), weights of evidence (Ozdemir 2011; Lee et al. 2012; Pourtaghi & Pourghasemi 2014), index of entropy (Al-Abadi et al. 2016), evidential belief function (Nampak et al. 2014), frequency ratio (Al-Abadi et al. 2016) and logistic regression model (Oh et al. 2011; Chen et al. 2018). These models can find a maximal factorization of the joint density of a set of random variables based on a set of joint observations of these variables. The multi-criteria analysis techniques are widely used in this research. The analytical hierarchy process (AHP) developed by (Saaty 1980) is one of the most popular models which have shown great ability to assess groundwater potential in different regions and have provided the benefit of simplifying the mathematical complexity of decision making (Machiwal et al. 2011; Rajasekhar et al. 2019). In recent years, many researchers have used approaches based on the use of remote sensing and GIS in combination with the AHP model for the assessment of groundwater potential in various arid and semi-arid regions (Arunbose et al. 2021; Doke et al. 2021; Sapkota et al. 2021; Ifediegwu 2022; Sajil Kumar et al. 2022).

Ajay Kumar et al (2020a) demonstrated that there is a strong correlation between borehole yields and groundwater potential index calculated using a GIS, Remote Sensing, and AHP based approach, at the Deccan Maharastra volcanic province level in India. Moreover, Al-Djazouli et al (2021b) used the coupling of GIS, Remote Sensing, and AHP to delineate potential groundwater areas in the Waddai area, Eastern Chad. The results of this research showed a great success of this approach,as well as its use in areas with arid climates, which is highly recommended by the authors. Abijith et al (2020a) presented the good accuracy (AUC = 0.75) of an approach that integrated GIS, remote sensing, and AHP in the assessment of groundwater potential in the Ponnaniyaru Tamil Nadu catchment in India. Furthermore, Rahmati et al (2015) developed an approach integrating GIS and AHP remote sensing to identify potential groundwater areas in the semi-arid region of Ghorve-Dehgolan, western Iran with an accuracy of 73%. The success of this type of approach in the assessment of groundwater potential in different arid and semi-arid regions on land has led us to apply it in the present study area, the region of Telmzoun situated in southern Morocco. The geo-hydrological factors that were chosen in this study are geology, distance to fault, slope, geomorphology, proximity to drainage network, drainage density, lineament density, and rainfall. This choice was based on an extensive literature review (Table 1) and through several studies results of hydrogeology experts. The main objective of this work is to evaluate the groundwater potentiality in the arid Telmzoun region, located in the southern part of Morocco, by developing a timely and low-cost prospective approach, using AHP in combination with GIS and Remote Sensing techniques, in order to orient future conventional prospecting campaigns in the study area.

Table 1. Literature on determining control factors for groundwater potential mapping

References	GL	DF	SL	GM	DD	DSD	DSL	RA
Ettazarini, 2020	*		*					*
Arabameri et al. 2020	*	*	*		*	*		*
Ajay Kumar, 2020	*		*	*		*	*	
Rajasekhar et al. 2019	*		*	*		*		
Çelik 2019	*		*	*			*	*
Al-Ruzouq et al. 2019	*	*	*	*	*	*	*	*
Khosravi et al. 2018	*	*	*		*			*
Boori et al.2018	*		*			*		
Mukesh Singh Boori, 2018	*			*		*	*	*
Adeyeye et al 2019	*		*		*	*	*	
Jenifer and Jha 2017	*		*			*	*	*
Thapa et al. 2018	*		*	*		*	*	*
Ghorbani Nejad et al. 2017	*	*	*		*	*		
Aouragh et al. 2017	*		*			*	*	

STUDY AREA

The present study focuses on the rural area of Telmzoun which is located in the southwest of Morocco, comprising an area of about 20.37 km^2 and situated between longitudes 10° 56' 53" and 10° 38' 53" West and latitudes 28° 56'50,698" and 28° 26'47,394" North (Figure 1). The elevation variation of the area is between 14 and 740 meters. Hydro-climatologically, the study area is located in the Draa watershed, which is characterized by an arid climate and the average monthly temperature varies between 20 and 25. In summer and between 15 and 20 °C in winter with low annual rainfall varying between 93 and 110 mm/year, the total population of the study area amounted to 2290 inhabitants in 2014. The main economic activities are camel breeding and subsistence cultivation. The access to groundwater in this area by the mainly rural population is limited due to its hydrogeological complexity. Therefore, the succession of drought years aggravated this situation and, consequently, waves of rural

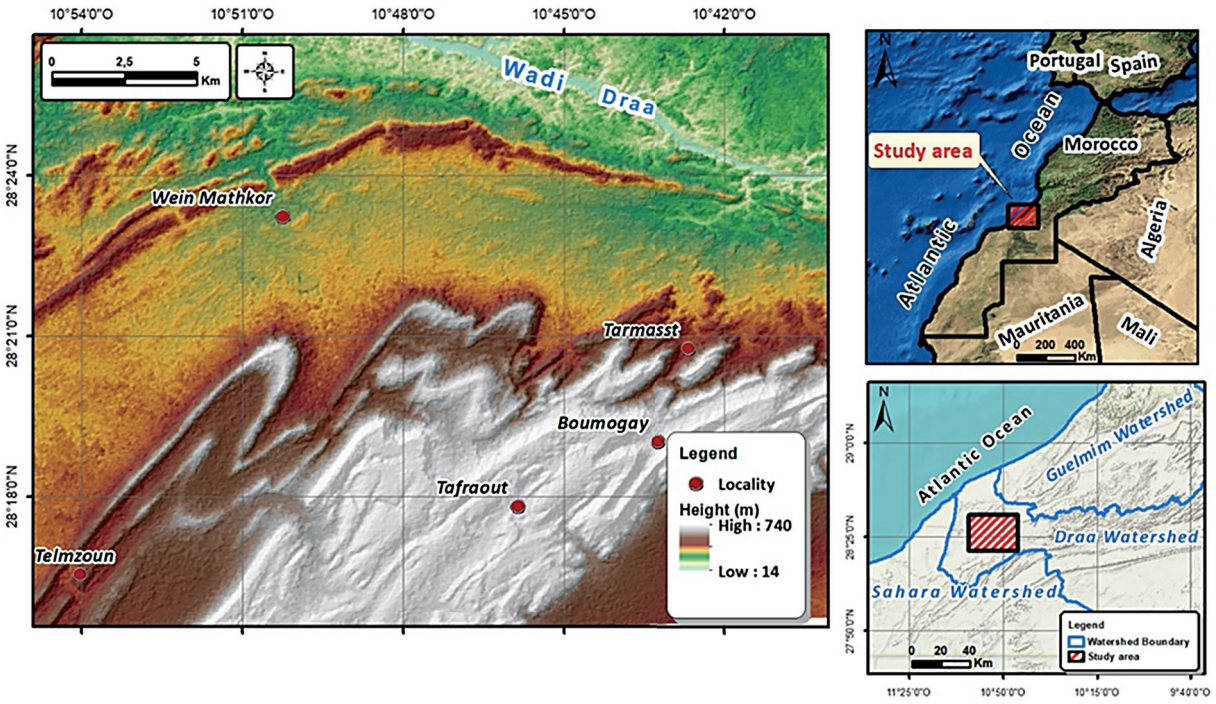

Figure 1. Geographical location map of the study area

exodus occurred. In response to this situation, the Moroccan government has launched several groundwater prospecting programs, in particular, the realization of high-cost exploratory surveys with a significant failure rate.

Geological and hydrogeological setting of the study area

The study area is located in the extreme southwest of the Western Anti-Atlas belt. It covers the southwestern part of the Low Draa inlier (Adiri et al. 2016). The substratum is constituted by metamorphic formations (gneiss and mica schists) of Paleoproterozoic age and is intruded by granitic bodies (El Hasnaoui et al. 2011). The latter generally consist of impermeable rocks and can only have a circulation of groundwater in their fractures or altered sites. This crystalline basement is surmounted by: (i) a Neoproterozoic cover, essentially represented by a volcano-detritic complex, rhyolites, ignimbrites, and andesites (Soulaimani et al. 1996), and is generally considered as impermeable formations, but may contain groundwater in the form of small aquifers located at the fault network and joints (Soulaimani et al. 1997), (ii) a sedimentary series of Infracambrian age (wine lees series), which includes limestones and dolomites (Soulaimani et al. 1997; El Hasnaoui et al. 2011).These carbonate formations are characterized by a good porosity and present a great hydrogeological interest. They constitute a seat of groundwater circulation that comes from the infiltration of rainwater or water drained by the rivers (Maloof et al. 2005) (iii) middle Cambrian outcrops in the south of the

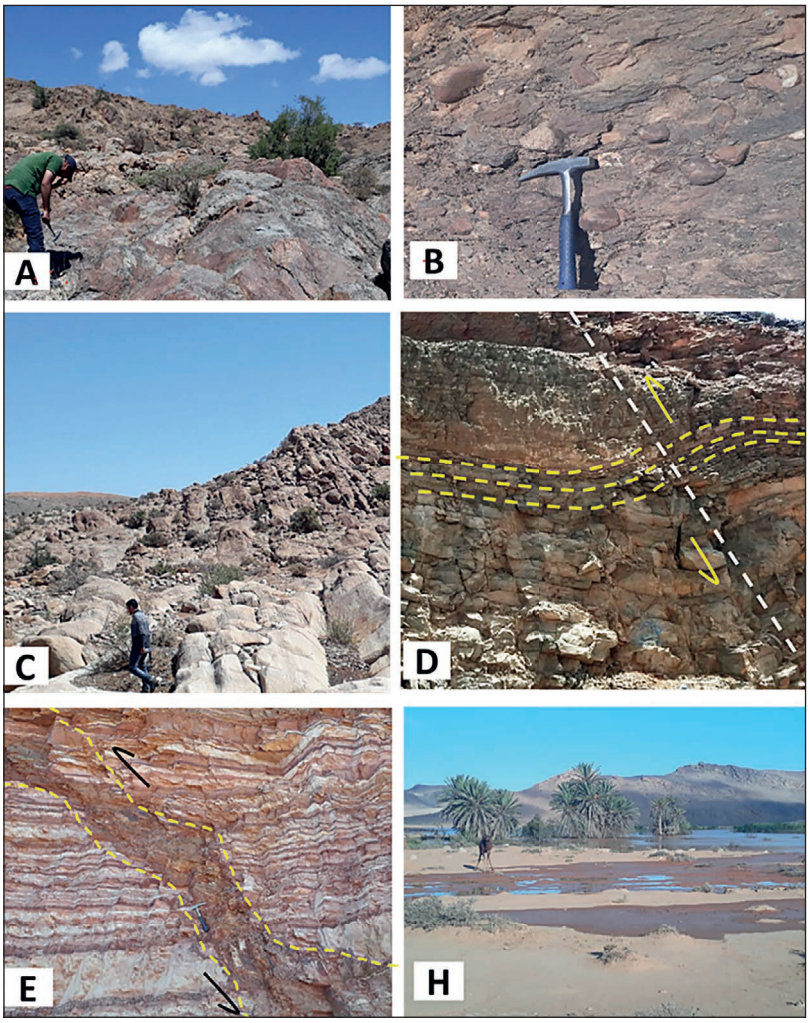

Figure 2. Photography of the outcropping geological formations in the study area; a) Granitic intrusion of Precambrian age; b) Volcano-detrital rocks of Neoproterozoic age; c) Limestone and dolomite of the Infracambrian (wine lees series); d) Folded and faulted pelitic series of the middle Cambrian; e) Ordovician sandstones with a fault corridor filled with clayey materials; h) Flood plain constituted by recent Quaternary alluvium

Low inilier. They are presented in the form of a series of folded sandstone-pelitic rocks that create depressions (internal Feija group); these rocks are considered to be moderately permeable. The formations of the Tabanit group consist of coarse-grained quartzites of middle Cambrian age that occur in a synclinal structure near Tafrouat and determine the main morphological ridges (Braunner et al. 2020). These formations are known by their fracture permeability and represent an important groundwater reservoir.The drainage of the contained water is assured by the rivers in cluses cut in its hard benches. (iiii) The Ordovician, essentially detritic, is constituted by the "External Feija" shales and crowned by the sandstone and quartzite of Jbel Bani. These thick and low permeability grounds do not present a significant hydro-geological interest. (iiiii) The recent formations of the Quaternary constitute alluvium, scree, alluvial cones, and calcareous crusts. Recent alluvial deposits fill the valleys and form alluvial aquifers that cover impermeable rocks with a significant thickness (Figure 2).

MATERIALS AND METHODS

The delineation of potential groundwater areas required a well-established approach that initiates with the collection of data and ends with the verification of the resulting map. Figure 3 shows the flowchart of the adopted methodology. The present study adopted the AHP method, consisting of eight factors that were selected for the geospatial mapping of groundwater after assessing many published works. To prepare the groundwater potential map, the indicators were aggregated using relative weights derived from AHP with input key hydrogeology experts.

Description of used data

The used data to prepare the thematic layers of the geo-hydrological factors are varied and extracted from different sources. They consist of the data of 41 drillings and 22 wells provided by the agency of the hydrological basins of Draa Oued-Noun and the geological maps of Alyoun Daraa and Telmzoun regions with the scale of 1/50 000 produced by the Direction of Geology at the Ministry of Energy and Mines in Morocco. In addition, the rainfall data for the period 2004–2014 of 20 meteorological stations were collected from the Guelmim Oued-Noun watershed agency.

Then, a set of satellite data have been downloaded; it is mainly a time series of annual precipitation estimates from 2004 to 2014 with Geotiff format of the product PERSIANN-CSS-CDR (Precipitation Estimation from Remotely Sensed Information using Artificial Neural Networks -Climate Data Record). This data has been downloaded from the https://chrsdata.eng.uci.edu website. Secondly, the Digital Elevation Model (ASTER DEM) was downloaded from the https://earthexplorer.usgs.gov website. Lastly, the Landsat OLI 8 (Operational Land Imager) satellite image scene acquired on 27-04-2019 was downloaded from the https://earthexplorer.usgs.gov website. Table 2 illustrates the source of the data utilized for the creation of the layers for each geohydrological Control Factor.

Process for preparing the geohydrological control factor layers

The preparation of thematic layers of different geohydrological factors requires the processing of the available satellite images, digitization of existing conventional maps in the study area, and the application of some statistical models.

Table 2. Geohydrological Control Factors and associated sources of the data set

Name of factor	Sources
Geology	Geological maps of Alyoun Daraa and Telmzoun regions, Morocco (Scale 1: 50 000)
Distance to faults	Geological maps of Alyoun Daraa and Telmzoun regions, Morocco (Scale 1: 50 000)
Slope	Prepared from ASTER DEM (USGS) (spatial resolution: 30 m)
Geomorphology	Derived from Landsat 8 OLI (spatial Resolution: 30 m) and ASTER DEM (spatial Resolution: 30 m).
Distance to the drainage network	Prepared from ASTER DEM (spatial Resolution: 30 m)
Drainage density	Prepared from ASTER DEM (spatial Resolution: 30 m)
Lineament density	Prepared from Landsat 8 OLI (spatial Resolution 30 m)
Rainfall	Prepared from a PERSIANN-CSS-CDR time series (0.04 degrees) and data measured at 20 metrological stations.

The first step consists in generating the thematic layer by digitizing the geological maps. Next, the slope, drainage proximity, and density raster layers have been generated through digital processing applied in ArcGIS 10.2 software on the Digital Elevation Model (ASTER DEM). The layer of Euclidean distance to faults was generated by digitizing the faults and shear zones represented in the geological maps and by using the Euclidean distance algorithm implemented in ArcGIS10.2. The lineament density layer was produced in two main steps; the first one is the automatic extraction of geological lineaments from a Landsat 8 OLI satellite image after applying various preprocessing and processing such as atmospheric correction by the DOS algorithm (Adiri et al. 2016) and geometric correction. The automatic extraction was applied on the principal component 1 (Adiri et al. 2017) (PC1), using the PCA Geomatica software. By the end of this step, the resulting lineament layer was subjected to a visual analysis to eliminate artifacts and was validated by the analysis of the directional Rose diagram. Therefore, the second step was the calculation of the lineament density in the Arc GIS 10.2 software. The geomorphology layer was produced by interpreting the Landsat 8 OLI satellite image and the Aster DEM, accompanied by field explorations. Subsequently, the annual rainfall layer was generated by using a polynomial model, which allowed estimating the rainfall measured by the satellite rainfall data (CCS-CDR PERSIANN), and the spatialization of this data was achieved by applying the Raster calculator algorithm implemented on ArcGIS 10.2 software.

Generation of normalized weights of geohydrological control factors using AHP

Weighting is the operation that served to assign a normalized weight to each geohydrological factor in the function of its influence on

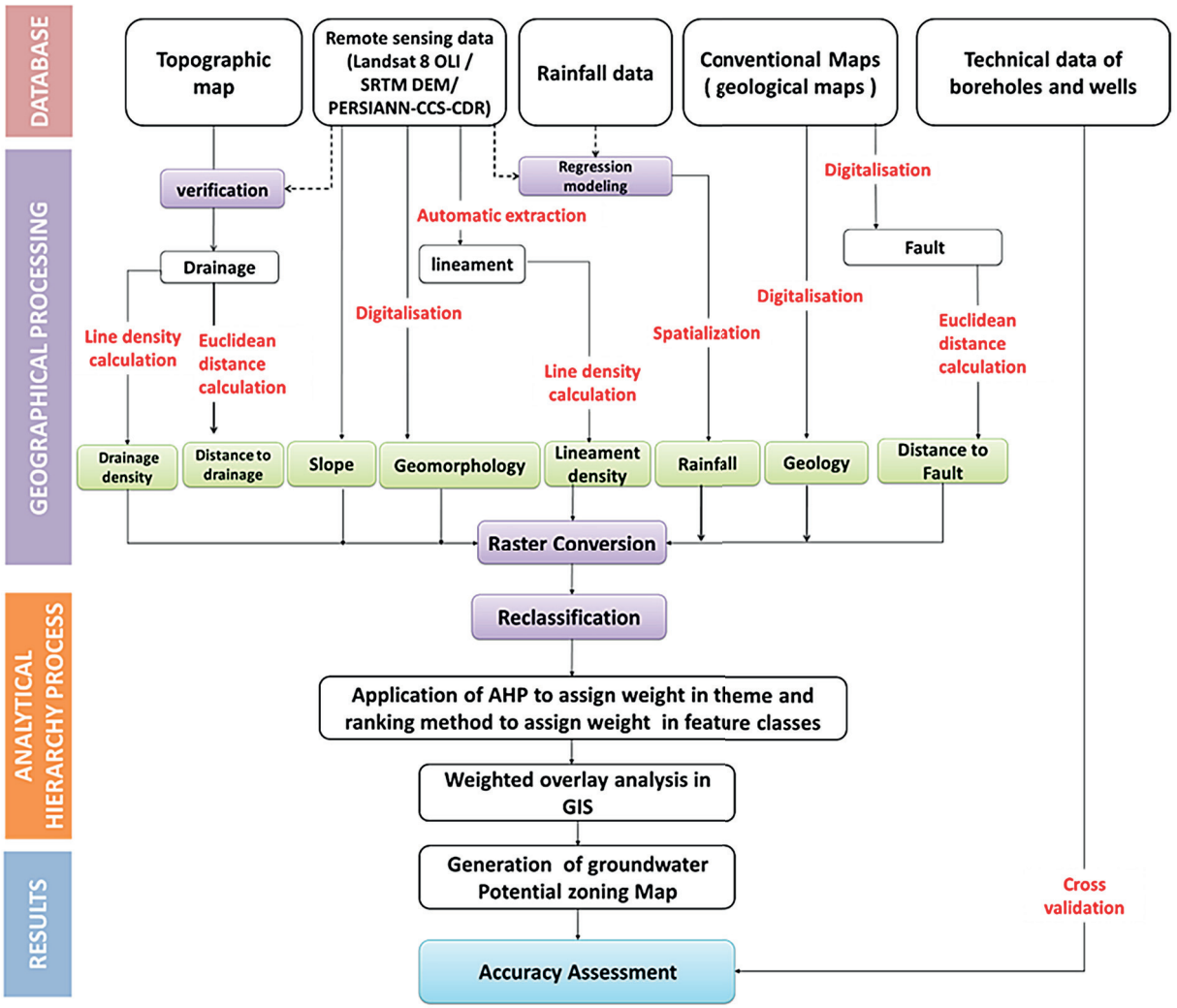

Figure 3. The methodology flowchart

groundwater occurrence (Erinjery et al. 2018). In our case, this operation was realized using the AHP model developed by (Saaty 1980). It consists of a matrix of pairwise comparisons between all the control factors (Table 3) where score 1 represents the equal influence and score nine represents the extreme influence of the parameters. According to the relative importance scale proposed by (Saaty 1980) (Table 4), this comparison includes opinions of hydrogeologists. Therefore, after establishing the pairwise comparison matrix, the normalized weight value of each control factor was calculated by normalizing the value of its eigenvector (i.e., dividing each eigenvector by their sum (Morjani & Abidine 2002)). In the end, we got eight normalized weights whose sum is equal to 1.

The coherence of the generated weights was assessed by using the method of Saaty (1980); this assessment is based on the calculation of a consistency ratio (CR). To achieve this task, two steps were followed (Shekhar and Pandey 2015):

- Step 1: Calculation of the coherence index (CI) by the following equation 1:

$$CI = \frac{\lambda max + n}{n - 1} \quad (1)$$

where: n – the number of used factors in the analysis; λmax – the maximum eigenvalue of the pairwise comparison matrix.

- Step 2: calculation of CR according to the following ratio formula 2:

$$\mathrm{CR} = \frac{\mathrm{CI}}{\mathrm{RCI}} \quad (2)$$

where: RCI is the random consistency index, whose values depend on the number of criteria selected, and it was obtained from the standard Saaty 1980 (Table 5).

If the CR value is lower than or equal to 0.10, the consistency of the matrix is considered acceptable and consequently the continuation of the analysis is possible. If the CR value is strictly greater than 0.10, it is necessary to review the pairwise comparison matrix to identify the causes of inconsistency and then correct them. If the CR is zero, it indicates a perfect level of consistency in the pairwise comparison (Fashae et al. 2014). In the case of the present study, for n = 8, CR is equal to 0.034; as this value is strictly lower than 0.10, this signified that the consistency level of the pairwise comparison matrix is acceptable (Saaty 1980).

Weighted superposition of control factors and generation of groundwater potential map

Through this step, the selected factors of influence were classified into ranges of values or

Table 3. Scale of relative importance developed by Saaty 1980

Control factors	GL	D.F	SL	GM	D.D	DSD	DSL	RA	Weight
Geology	1	1	1	1	2	2	3	5	18.6%
Distance to faults		1	1	1/2	3	2	2	5	17.6%
Slope			1	1	3	1	2	3	16.1%
Geomorphology				1	1	1	1	3	14.9%
Distance to drainage					1	1	1	3	9.3%
Drainage density						1	1	2	10.4%
Lineament density							1	2	9.0%
Rainfall								1	4.2%

Table 4. Matrix of pairwise comparisons between the control factors

Scale	1	2	3	4	5	6	7	8	9
Importance	Equal	Weak	Moderate	Moderate plus	Strong	Strong plus	Very strong	Very, very strong	Extreme

Table 5. RCI values for different numbers of criteria (Staay 1980)

Number of criteria (n)	1	2	3	4	5	6	7	8	9	10
RCI values	0	0	0.58	0.90	1.12	1.24	1.32	1.41	1.45	1.49

Table 6. Standardization table of geohydrological control factors

No.	Control factors	Entity/value range	Qualifications	Score attributed	Weight
1)	Rainfall (mm/an)	93–96	Very low	1	0.042
		96–99	Low	2	
		99–102	Low	3	
		102–105	Moderate	4	
		105–109	Very moderate	5	
2)	Lineaments density (km/km²)	0–0.32	Very low	1	0.09
		0.32–0.8	Moderate	4	
		0.8–1.3	Very moderate	6	
		1.3–2.01	Strong	8	
		2.01–3.35	Very strong	10	
3)	Distance to drainage (m)	0–300	Very strong	10	0.093
		300–600	Very moderate	6	
		600–900	Moderate	4	
		900–1200	Low	2	
		> 1200	Very low	1	
4)	Slope (degree)	0–5.8	Very strong	10	0.161
		5.8 à 11.4	Strong	8	
		11.4 à 18.3	Moderate	4	
		18.3 à 27	Low	2	
		> 27	Very low	1	
5)	Geomorphology	Denudative hills, residual hills (Small)	Low	2	0.149
		Residual hills (large)	Moderate	4	
		Highly eroded peneplains, intermontane valley	Very moderate	5	
		Less eroded peneplains	Strong	8	
		Piedmont / Valley floor	Moderate	3	
		Valley filling / filled valley	Very strong	10	
		Ridge–type structural hills	Very low	1	
		Flood plains, plain	Very strong	10	
6)	Distance to faults (m)	0–500	Very strong	10	0.176
		500–1000	Strong	8	
		1000–1500	Moderate	4	
		1500–2000	Low	2	
		> 2000	Very low	1	
7)	Drainage Density (km/km²)	0–0.76	Very strong	10	0.104
		0.76–1.5	Strong	9	
		1.5–2.3	Very moderate	6	
		2.3–3.0	Moderate	4	
		> 3.00	Low	2	
8)	Geology	Alluvium	Very strong	10	0.186
		Quartzite in large benches, Limestone, dolomite and conglomerates	Strong	8	
		Volcanodetritic rocks, pelite	Moderate	4	
		Quartzitic sandstone Epiclastic rocks and pelite, Limestone crusting	Low	2	
		Shale, volcanic rocks, Acidic magmatic rock	Very low	1	

particular entities according to their common characteristics concerning the occurrence of groundwater. Subsequently, a score was attributed to each class based on their importance in the infiltration and retention process of groundwater. A rating scale ranging from 1 to 10 was used for this assessment, a score of 10 was assigned to classes of " very strong " importance, while a score of 1 was assigned to classes of "very low" importance, and the intermediate values were assigned to the intermediate classes as illustrated in Table 6.

The Groundwater Potential Index (GWPI) layer was generated by a weighted overlay of all standardized influence factors using the Raster Calculator option of ArcGIS 10.2; this overlay is mathematically written by the following equation 3:

$$GWPI = (C_{GL}.\omega_{GL}) + (C_{DF}.\omega_{DF}) + (C_{sp}.\omega_{sp}) + \\ +(C_{GM}.\omega_{GM}) + (C_{DD}.\omega_{DSD}) + (C_{DSD}.\omega_{DSD}) + \\ +(C_{DSL}.\omega_{DSL}) + (C_{RA}.\omega_{RA}) \quad (3)$$

where: C_{GL} is the geology raster layer;
C_{DF} is the distance to fault raster layer;
C_{sp} is the slope raster layer;
C_{GM} is the geomorphology raster layer;
C_{DD} is the distance to drainage raster layer;
C_{DSD} is the drainage density raster layer;
C_{DSL} is the lineament density raster layer;
C_{RA} is the annual rainfall raster layer;
ω is the normalized weight associated with each factor.

The resulting groundwater potential index was classified into five classes: very low, low, moderate, high and very high groundwater potential areas, using the natural breaks method.

Verification of the groundwater potential index

The verification of the resulting groundwater potentiality index is an essential step for testing the performance of the developed approach, as well as for quantifying the accuracy of the model used. In fact, the use of technical data from existing boreholes and wells is essential. In this study, the data of the performance of 41 water points were used, so a statistical summary of the latter is presented in Figure 4 and Table 7.

In order to verify the accuracy of the final groundwater potential map, the measured yield rates of the water points (boreholes) were grouped into five classes as shown in Table 8. Then, the yield classes of the water points were overlaid on GWPI to verify the correspondence between the yield class of a water point and the groundwater potential class derived from the GWP map.

A remark of 'agree' means that there is a concordance between the measured yield class and the potentiality class of GWPM. On the other hand, a remark of 'disagree' means that there is a

Table 7. Water point yield statistics used for GWP verification

N total	Depth(m)	Water yields (l/s)					
	Mean	Mean	Standard Deviation	Sum	Minimum	Median	Maximum
41	88.6	2.34707	3.24144	96.23	0	1.2	13

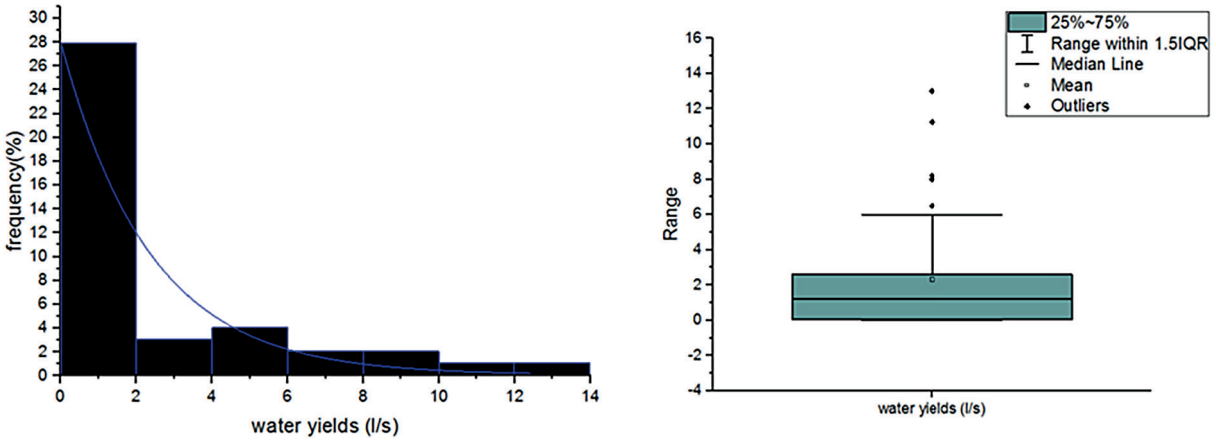

Figure 4. Histogram and box plot of water point yields used for GWPI verification

Table 8. Water point yield ranking

Yield interval (l/s)	Yield classes
0–0.2	Very low
0.2–0.8	Low
0.8–1.5	Moderate
1.5–4	High
>4	Very high

discordance. This method allowed us to quantify the accuracy of the resulting potentiality map using the following formula (4) (Das & Mukhopadhyay 2020; Sajil Kumar et al. 2022):

$$\text{GWPM Accuracy}(\%) = \\ = \frac{\text{number of agreement samples}}{\text{total number of water points}} \times 100 \quad (4)$$

A second method of verification is used in order to confirm the accuracy obtained by the method described above; it is a frequently used method named the ROC curve (Receiver Operating Characteristic) and the Area Under the (AUC) (El Jazouli et al. 2019). The ROC method is widely used to estimate the validity of a model since it predicts the location of the case (occurrence) of a class by comparing an image of adequacy, illustrating the probability where this class occurs, and a Boolean image showing where this class exists.

RESULTS AND DISCUSSION

Geological map

Geology is considered as the most important criterion to assess the groundwater potential, as it directly governs the infiltration process, storage and circulation of groundwater, which depends on the porosity and permeability of the rock formation (Aggarwal et al. 2019). The geological layer of the study area was derived from the conventional geological map of ~~A~~youn Daraa and Telmzoun regions with the scale 1/50 000. Alluvium, quartzite, limestone, dolomite, conglomerates, pelite, volcanodetritic rocks, shale, volcanic rocks, and acidic magmatic rocks are the geological formations that were found in the study area (Figure 5). They were classified according to their degree of permeability; the very strong class was assigned to the Alluvium formation, and the very low class was assigned to shale, volcanic rocks, and acidic magmatic rocks, while the other formations found were classified as strong, moderate, and low.

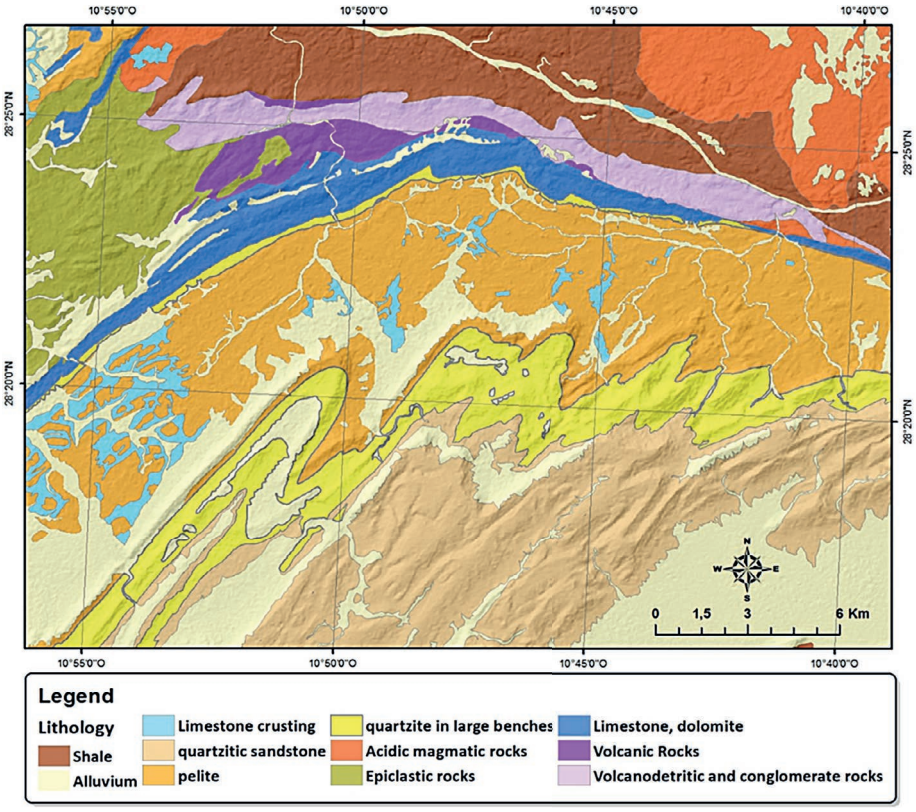

Figure 5. Geological map of the study area

Faults proximity map

Faults are geological structures that constitute discontinuities in the geological formations, which are often filled by altered and very permeable materials with high secondary porosity and assure a good infiltration of rainwater. They could constitute groundwater reservoirs by developing an alteration zone around them. Several previous studies have shown that the yields of boreholes located in zones close to faults are significant, and that the yield increases with the increasing depth and thickness of the alteration zone (Ettazarini & El Jakani 2020). Therefore, the mapping of faults and their peripheries is very useful in the identification of potentially productive regions, as well as in the discovery of new reservoirs in fractured zones.

The study area is characterized by the presence of a system of faults in the Precambrian basement of the Low Draa and formations of the Middle Cambrian, including sandstone-pelitic formations; this system is mainly oriented to the north 45° (SOULAIMANI et al. 1996) (Figure 6).

The Euclidean distance layer to faults was calculated using ArcGIS10.2 software to determine the areas that are close to the fault network (Figure 7). 500 meters from the fault system was considered as an area of high groundwater potential, while an area greater than 2000 meters from the fault was considered as an area of very low potential. Five buffer zones were identified, (0 to 500), (500 to 1000), (1000 to 1500), (1500 to 2000) and (>2000), which cover areas of 4.95 km², 4.04 km², 3.08 km², 2.4 km² and 5.88 km² respectively.

Slope map

Slope is a topographic parameter that directly governs the behavior of surface water flow and the process of water infiltration to the subsoil. This means that in regions with low slopes, water flow is very slow, which gives more time to rainwater to infiltrate, while regions with steep slopes are very favorable for rapid water flow, therefore leaving less time for rainwater to infiltrate (Das & Mukhopadhyay 2020). In other words, infiltration is inversely proportional to the slope degree (Rahmati et al. 2015). The resulting slope map (Figure 8) shows variates from 0 to 57, which led us to classify them into five intervals. Class 1 (0–5°) corresponds to the class with good infiltration conditions, constitutes a percentage of 35% of the total surface of the study area, and is considered as an area with good groundwater potentiality. Class 2 (5–10°) represents almost 33% of the total area, is described as an areas of good infiltration conditions, and is then automatically judged as good in terms of groundwater potentiality. Class 3 (10–20°), representing almost 17.8% of the study area, is described in terms of groundwater occurrence as moderate to low. Finally, class 4 (20 to 30) and class 5 (>30) indicate high

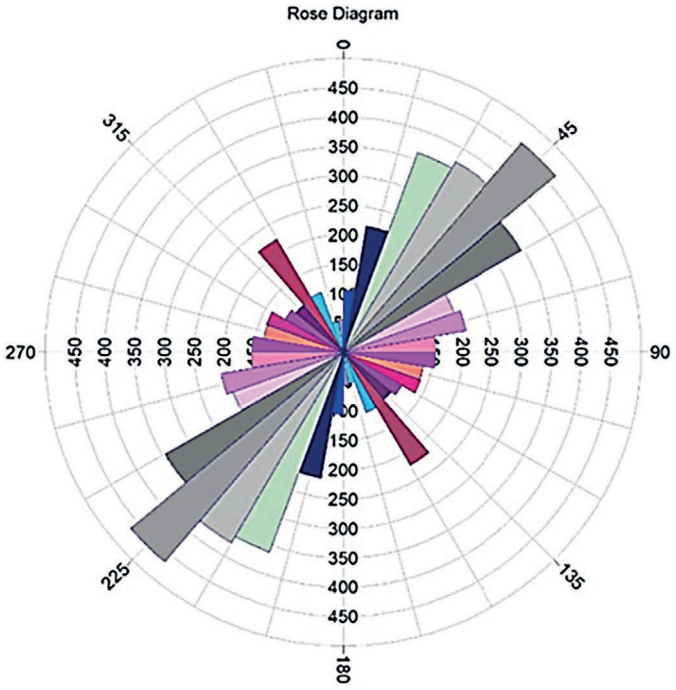

Figure 6. Rose diagram of fault orientations in the study area

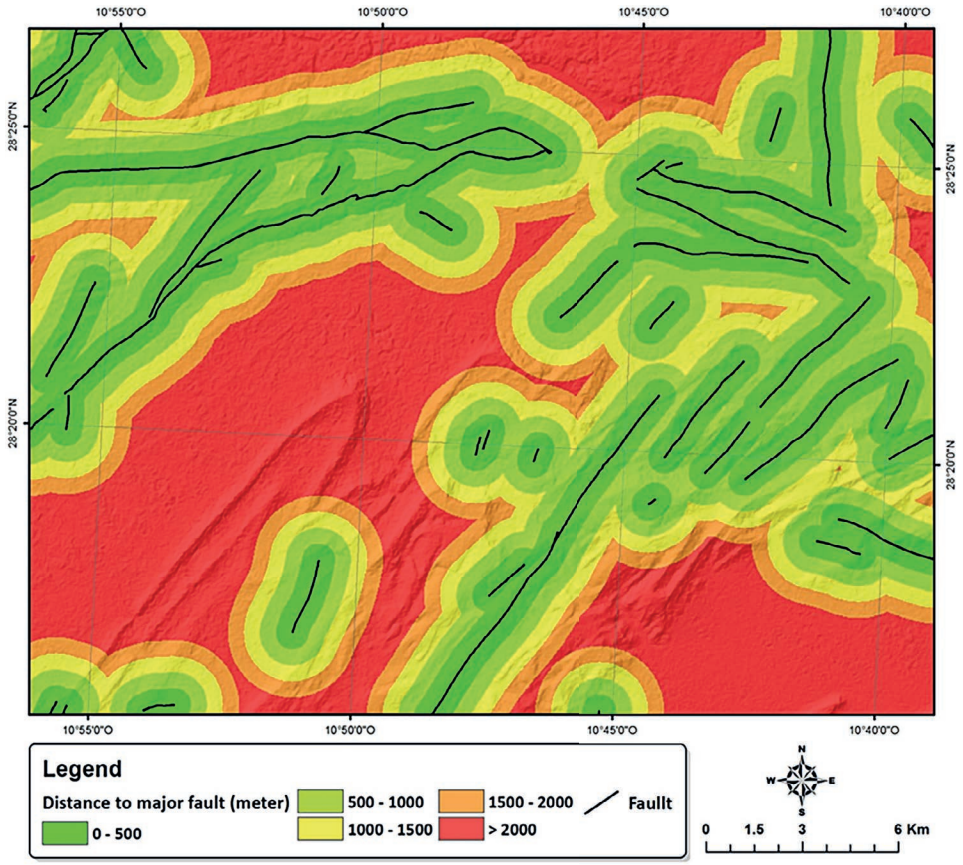

Figure 7. Faults proximity map of the study area

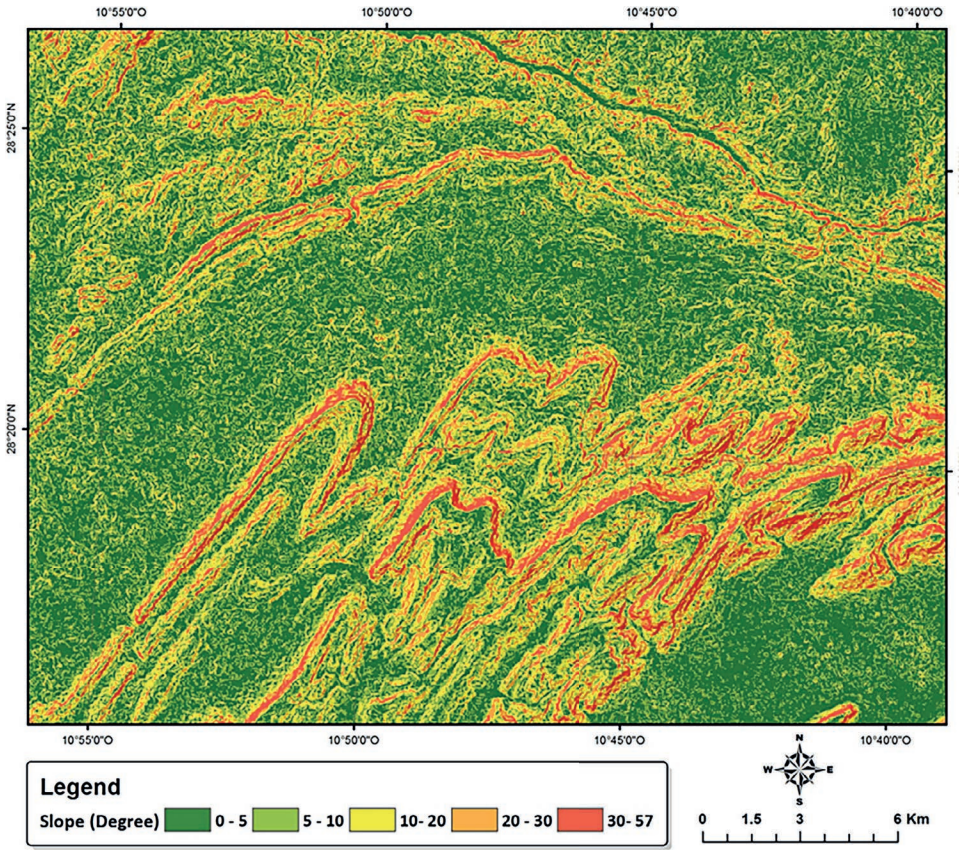

Figure 8. Slope map of the study area

and very high slope areas, which constitute 10% and 4.4%, respectively, of the total study area, and were considered as low to very low groundwater potentiality.

Geomorphology map

Geomorphology characterizes the landform and its topographic evolution (Ajay Kumar et al. 2020), which significantly influences various hydrological and hydrogeological processes, specifically runoff, water infiltration and the aquifer recharge process (Abijith et al. 2020). In this study, ten main geomorphological units were identified in (Figure 9); structural hills/ridges, shallow weathered peneplains and moderately weathered peneplains are the major geomorphic features in the study area.

Drainage proximity map

The distance from the hydrographic network is an important parameter in the exploration of groundwater because the areas closest to the rivers are often characterized by the presence of alluvial layers that are very permeable and with sufficient thickness to store groundwater; these layers are fed from both sides during periods of flooding, either naturally or intensively by the use of weirs on the rivers. Several researches have approved that, in the buffer zone 300 meters from the drainage network, the probability of existence of small productive alluvial layers is high (Benjmel et al. 2020).

In this study, the map of proximity to the hydrographic network (Figure 10) showed five classes of distance: (0 to 300), (300 to 600), (600 to 900), (900 to 1200), (1200 to 1500), and (1500 to 1800), which cover respectively 47.6%, 33.3%, 15.4%, 3.3% and 0.4% of the total surface of the study area. The areas that are in the range of 0–300 m are very responsive and are considered very good in terms of groundwater potentiality.

Drainage density map

Drainage density is one of the major determinants of groundwater occurrence; it is an inverse function of infiltration (Rahmati et al. 2015). This means that an area with low drainage density results in increased infiltration and decreased surface

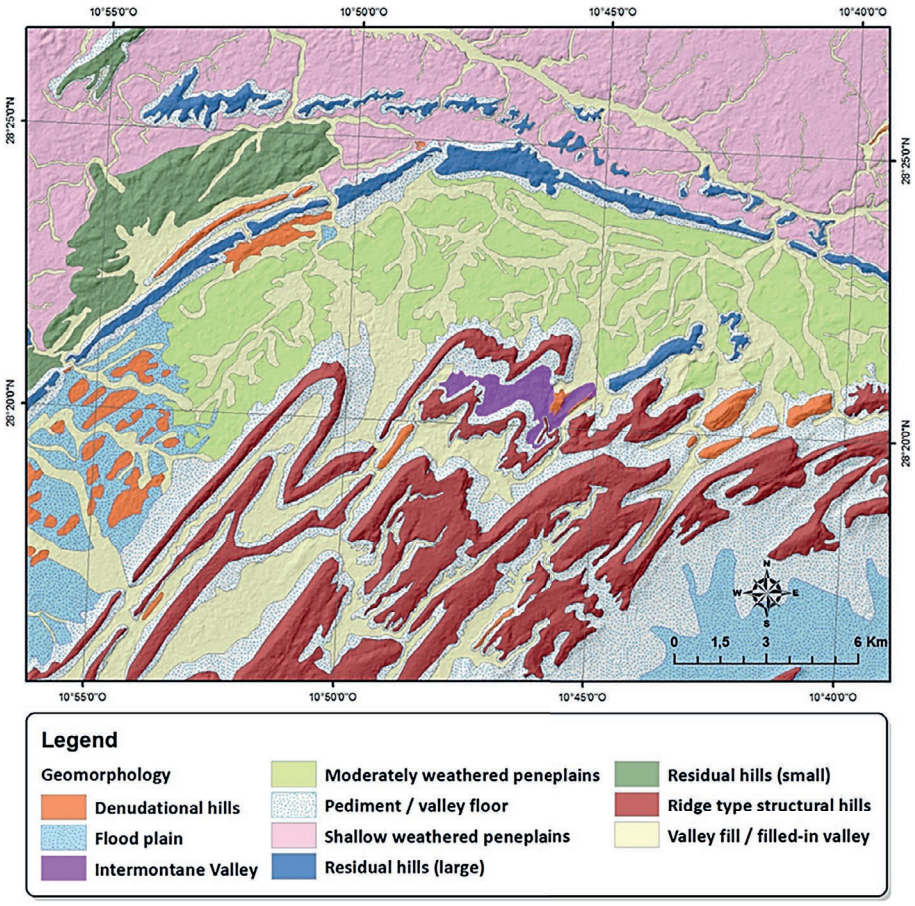

Figure 9. Geomorphology map of the study area

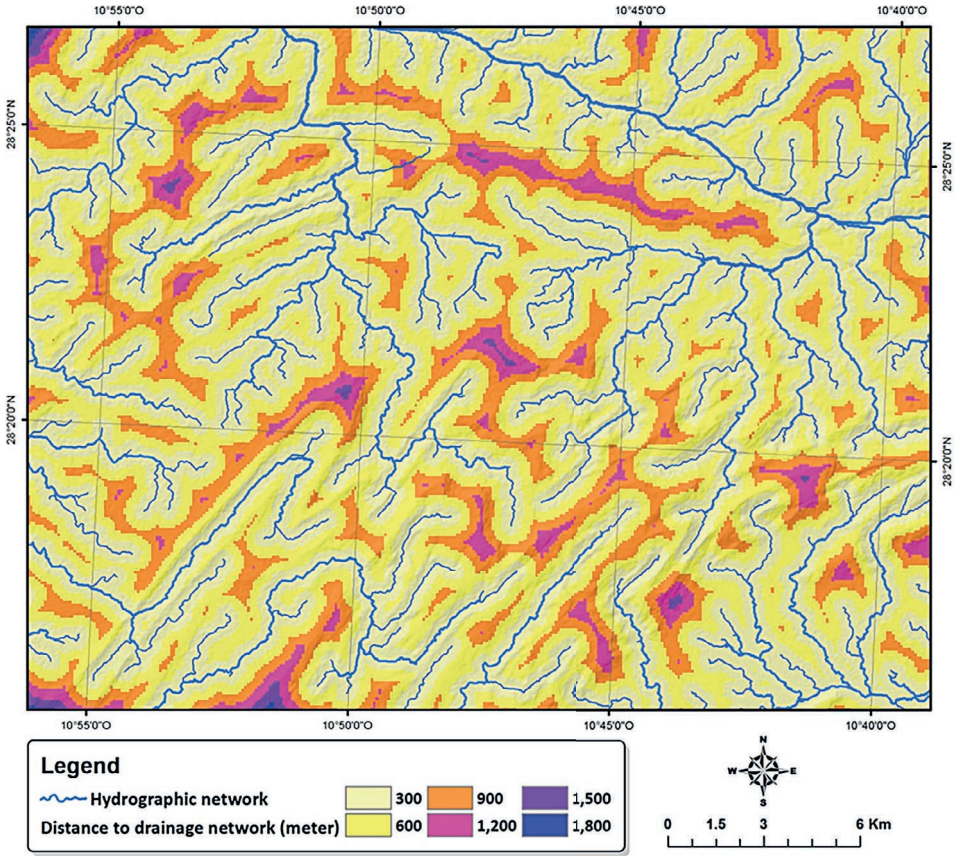

Figure 10. Drainage proximity map of the study area

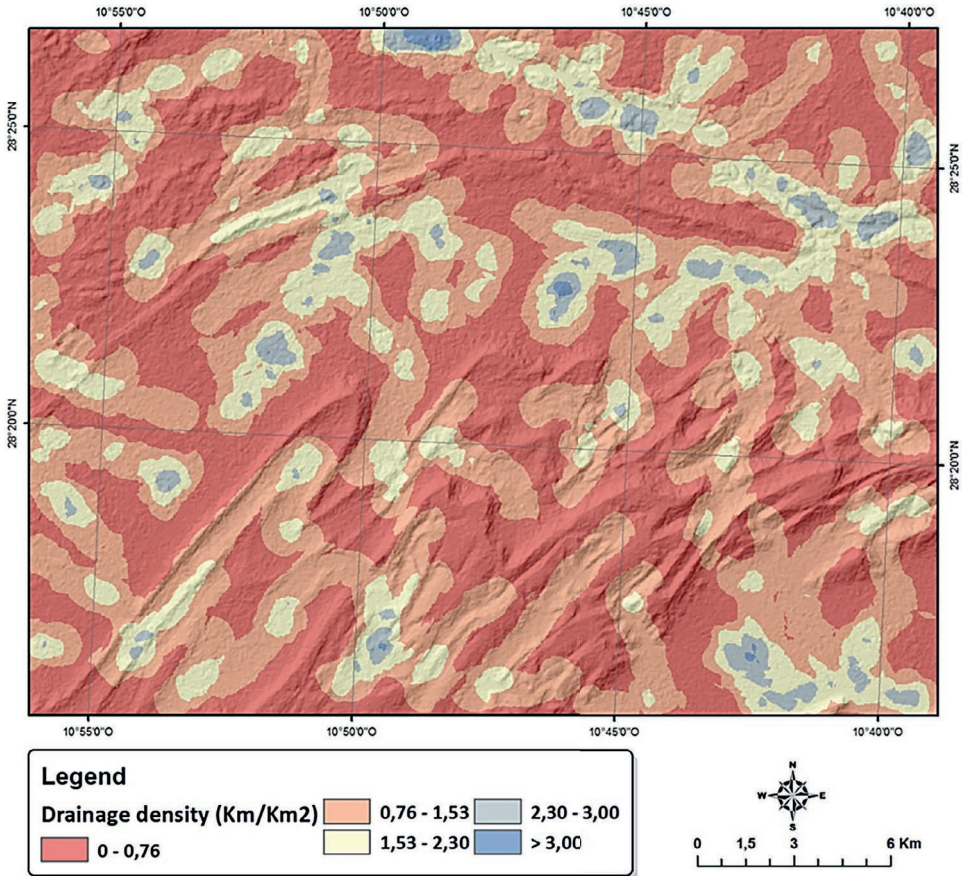

Figure 11. Drainage density map of the study area

runoff. So areas with low drainage density are suitable for groundwater development (Magesh et al. 2012). The drainage density in the current study is varying from 0 to 3.75 km/km2 (Figure 11); it was classified into five intervals: (<0.76 km/km^2), (0.76–1.50 km/km^2), (1.50–2.3 km/km^2), (2.3–3 km/km^2), and (>1.00 km/km^2), cover respectively 42.5%, 39%, 15.9%, 2.6%, and 0.2% of the study area. Therefore, a higher score was given to lower drainage density areas and lower scores were given to densely drainage areas (Table 6).

Lineament density map

Lineaments are linear or curvilinear structures that correspond to natural objects of tectonic and geomorphological origin namely faults, facies boundaries, rectilinear drainage zones, valleys, and ridges (Adiri et al. 2017; Jellouli et al. 2021); these structures are characterized by good permeability. Recently several authors have shown that areas of high lineament density generally have a high success rate of boreholes (Ajay Kumar et al. 2020; Sapkota et al. 2021). The lineament density layer map of the study area shows an orientation identical to that of the faults (North 45°) as shown in Figure 12.

The resulting lineament density map (Figure 13) was classified into five classes, (0–0.32), (0.32–0.86), (0.86–1.36), (1.36–2.01) and (>2.01), covering a percentage of: 45%, 29.5%, 12.3%, 9.5 and 3.5%, respectively, of the overall study area. The high density of lineament is located at the overlapping front between the buttonhole of the lower Draa and the sedimentary cover, this area is characterized by the outcrop of limestone Infracambrian monoclinal layers. Good density is also found in the Precambrian terrain; these areas are generally considered as areas of very high groundwater potential. The areas of very low density correspond to the alluvial plains of low tectonic activity; the latter are considered as areas of low groundwater potential from the point of view of lineament density.

Rainfall map

Precipitation is the main source of freshwater that can be percolated to aquifers, or runoff into streams, depending on the topographic conditions of the receiving surface; it is also considered the main source of aquifers recharge (Maity & Mandal 2019). Numerous previous researches have shown that there is a positive correlation between rainfall values and the degree of groundwater potentiality (Adiat et al. 2012).In this study, the annual rainfall map showed five main classes, namely 93–96 mm/year, 96–99 mm/year, 99–102 mm/year, 102–105 mm/year, and 105–109 mm/year (Figure 14). The areas with an annual average of 93–96 mm of precipitation are considered very low for groundwater potential, while

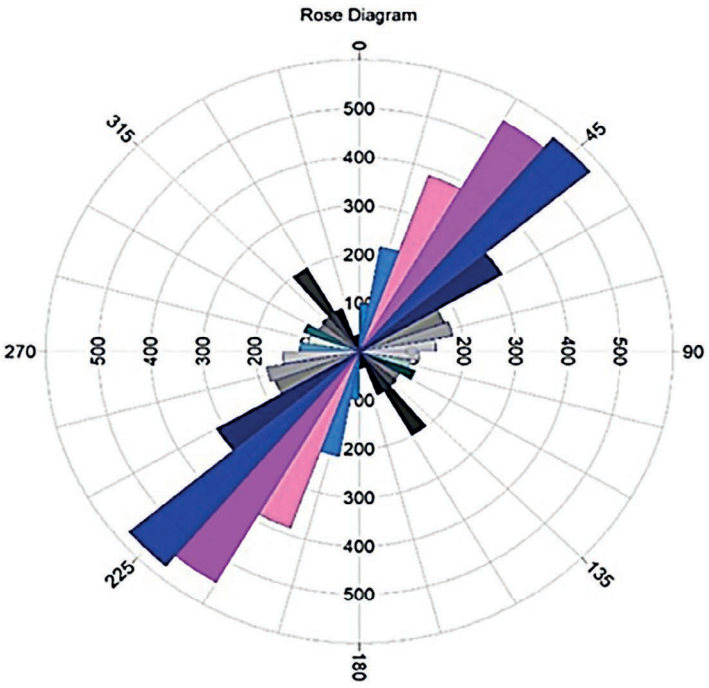

Figure 12. Rose diagram of the lineaments orientations in the study area

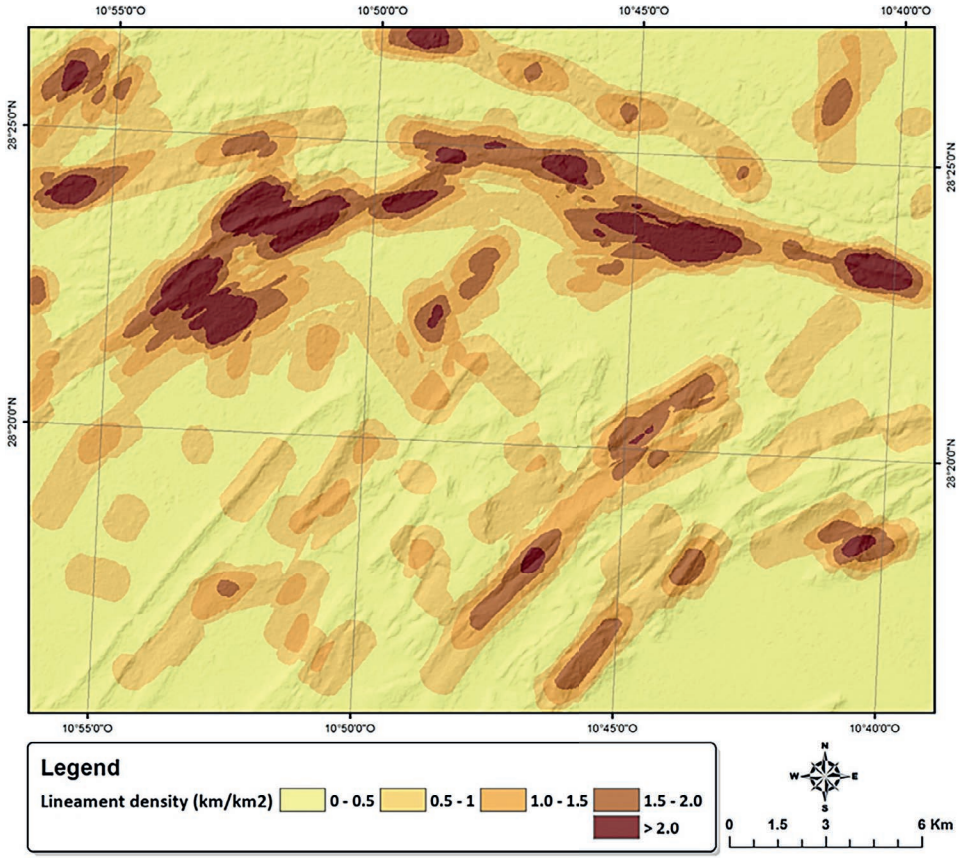

Figure 13. Lineament density map of the study area

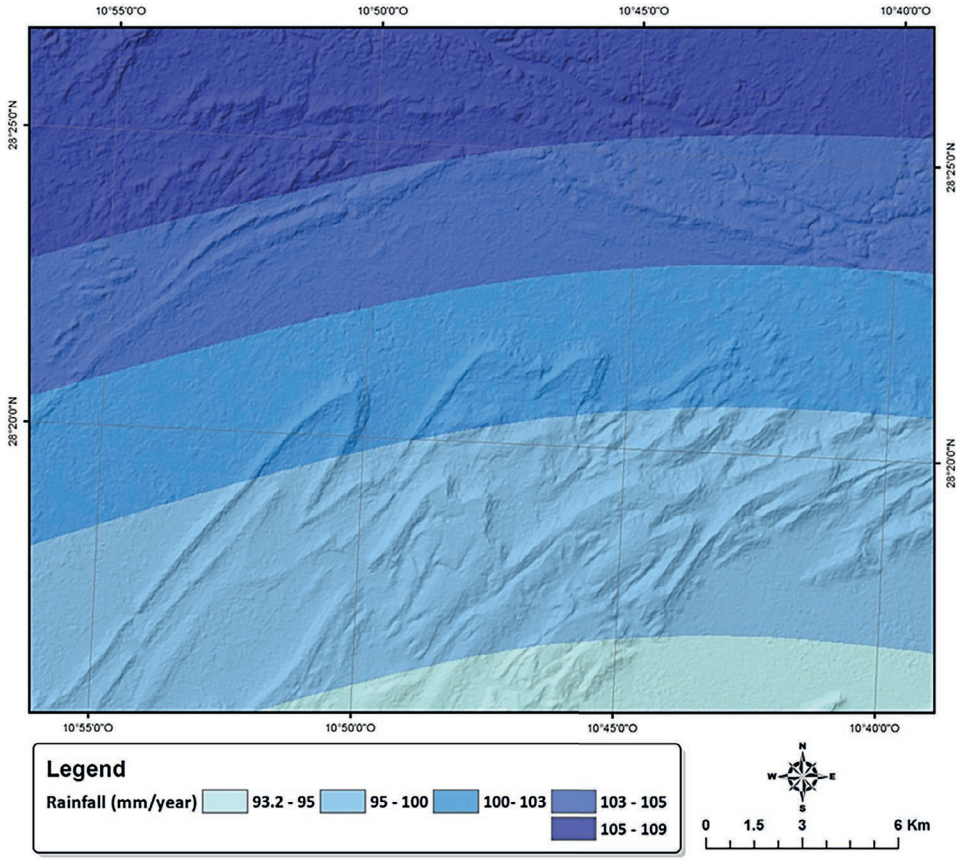

Figure 14. Rainfall map of the study area

the areas with an annual average of 96–99 mm/year, 99–102 mm/year, and 102–105 mm/year are considered low, and finally the areas with a value between 105–109 mm/year are considered moderate in terms of groundwater potentiality.

Groundwater potential map (GWPM)

By using the AHP method to find the relative weight and priority of individually factor, a groundwater potential map was prepared overlaying eight factors. The resulting groundwater potential map (Figure 15) discriminated between five zones, "very low", "low", "moderate", " high", and "very high". The "very low" and "low" groundwater potential zones are in the southeastern, southwestern, and northern parts of the study area. They cover an area of 2.4 km^2 and 4.17 km^2 respectively, or 32.4% of study area, and they correspond to ridges and domes of steep slopes as well as areas of impermeable rocks, where almost all conditions that favor runoff are met.

The "moderate" class covers an area of 6.06 km^2, about 30 % of the study area, and corresponds to areas of moderately permeable rocks and slope between 5° and 18°, where the density of drainage is strong; these conditions are very favorable for runoff, but may have small pockets of water that is stored within permeable sediments, especially in the case of light rainfall. The zones of "high" groundwater potential cover an area of 5.53 km^2 (27.2%) and correspond mostly to alluvial plains and valleys filled with very permeable materials and low slopes, where infiltration is very important, especially in this area, which is characterized by an arid climate and most of the its rainfall has been light. The zones of very high potentiality are located in the northeastern and northwestern parts of the study area; they cover an area of 2.14 km^2 or 10.5% of the study area. The "very high" potential of groundwater in these areas is mainly due to the presence of fault corridors, geological formations of high permeability such as Infracambrian limestone in the shallow slope areas, where almost all conditions for infiltration are met.

Validation of the GWPM map of Telmzoun

The accuracy of GWPM verification is important for decision makers. The results of the verification methods are presented below. First of all, a scatterplot was drawn by the flows of the water

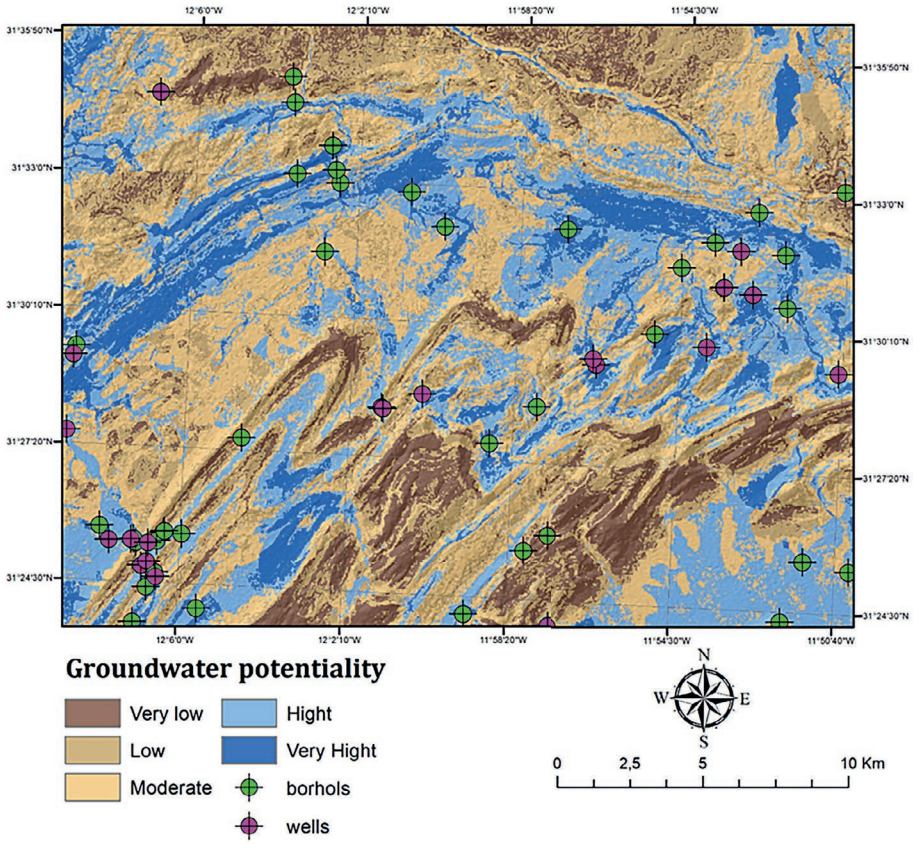

Figure 15. Groundwater potential map of the Telmzoun area (GWPM)

points according to the GWPI values and showed that there is more or less a non-linear correlation. We notice that the most important yields correspond to high values of GWP index, while the majority of the dry water points or those having low yields correspond to low values of GWP index (Figure 16). The accuracy of this map, according to the first method described in this paper, is 73.17%, with 30 as the number of samples in agreement, and 41 as the total number of samples used.

$$\text{GWPM Accuracy}(\%) = \frac{30}{41} \times 100 = 73.17\%$$

Validation of the GWP map via analytical hierarchy model was done by applying the Receiver Operating Characteristics (ROC) curve which has been widely used recently by several authors (Arumugam 2016; Dar et al. 2021; Pande et al. 2021). The area under curve (AUC) value of accuracy was 0.755; the analysis revealed that the global success rate of the groundwater map is 75.5% (Figure 17). It can therefore be deduced that the approach used in this study showed good accuracy in groundwater potential mapping (>70%). Many researchers also estimated the influence of the geomorphological, hydrological, lithological and relief factors in

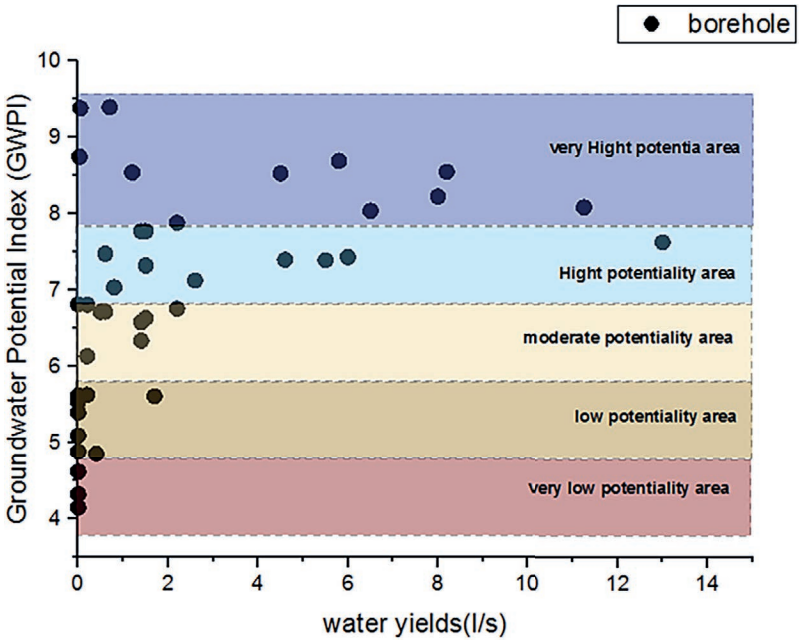

Figure 16. Scatterplot, GWP index values versus measured yields

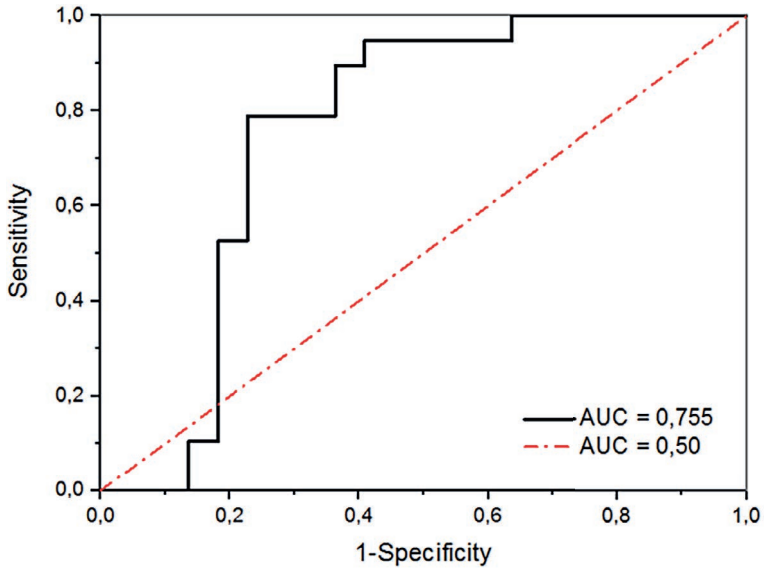

Figure 17. Receiver operating characteristics (ROC) curve of the GWPM

the groundwater potential. For instance, Patra et al 2018 asserted that geology had the strongest influence on groundwater potential in the alluvial plains of India. Similarly, for the semi-arid region in Botswana, Lentswe & Molwalefhe 2020 revealed that lithology has been the most important factor for groundwater potential. Like the present study, Das & Pal 2019 compared the frequency

Table 9. Verification table of the correspondence between the measured borehole yield classes and the estimated groundwater potential class

No	Locality	Lambert coordinates		Total depth (m)	Borehole yield (l/s)	Yield class	GWP class	Correspondence remark
		x(km)	*y*(km)					
1	Aghouinem	-25,700	152,600	85	1.5	High	High	Agree
2	Aouyi	-17,700	152,750	80	0.4	Low	Low	Agree
3	Aoyi	-16,900	154,800	72	2.2	High	High	Agree
4	Tilemzoune Centre	-39,240	154,455	80	6.0	Very high	High	Agree
5	Ouin Mdkour	-34,366	170,634	100	0.6	Low	High	Disagree
6	Tuizemzame	-41,900	162,300	100	0.5	Low	High	Disagree
7	Maarada	-39,993	152,743	80	11.25	Very high	Very high	Agree
8	Tanoulmi	-27,700	158,900	82	0.2	Low	Moderate	Disagree
9	Tiflfal	-19,600	164,250	100	1.7	High	Low	Disagree
10	Tiflfal(aval)	-17,468	165,365	90	0.7	Low	Very high	Disagree
11	Tarmest	-24,000	161,600	90	0.03	Very low	Very high	Disagree
12	Megsem El Fernane	-37,800	153,200	100	8.0	Very high	Very high	Agree
13	Tiflahine	-39,871	155,500	71	1.4	Moderate	Moderate	Agree
14	Lahouid	-38,300	155,800	62	13	Very high	High	Agree
15	Reg Ouin Kora	-41,120	156,104	98	1.4	Moderate-high	High	Agree
16	Oued Rtimi	-30,356	167,543	100	1.5	High	High	Agree
17	Tuihricht	-39,533	153,939	100	2.2	High	High	Agree
18	Lahouid	-38,920	155,831	120	2.6	High	High	Agree
19	Lahouid	-36,222	159,104	120	4.6	Very high	High	Agree
20	Khenig ali	-21,970	162,660	75	0.05	Very low	Very high	Disagree
21	Ikhalwa	-26,068	160,157	60	0.2	Very low	Moderate	Disagree
22	Tamalihat	-19,895	165,810	100	1.4	Moderate	Moderate	Agree
23	Oued Rtimi	-29,217	166,347	120	1.5	Moderate	Moderate	Agree
24	Tafraout ait oussa	-15,425	167,522	66	0	Very low	Very low	Agree
25	Ouin Mdkour	-34,431	171,517	60	0	Very low	Low	Agree
26	Khenig massoud	-34,613	173,799	79	0	Very low	Low	Agree
27	maarada	-27,812	173,561	80	0.2	Very low	Low	Agree
28	Zaouiat ait oussa	-15,327	154,450	100	0.6	Low	High	Disagree
29	Tafraout	-25,691	155,722	75	0	Very low	Very low	Agree
30	Tafraout	-28,610	153,000	60	0	Very low	Low	Agree
31	Tafraout (AgouinemII)	-26,530	155,204	100	0	Very low	Very low	Agree
32	Aftissat	-34,295	168,182	120	8.2	Very high	Very high	Agree
33	Oum lagliaa	-18,055	166,506	80	5.8	Very high	Very high	Agree
34	Hassi arsen	-24,943	166,267	100	1.2	Very high	Very high	Disagree
35	Aouint ighouman	-17,017	163,145	100	0.8	High	High	Agree
36	Rbyeb	-43,142	164,553	70	0	Very low	Low	Agree
37	Ouin Madkour	-33,353	165,496	100	0	Very low	Low	Agree
38	Tarmest	-21,043	164,945	100	0	Very low	Moderate	Disagree
39	Azogagh	-32,817	167,858	90	4.5	Very high	Very high	Agree
40	Lahouid lahmer	-32,948	168,305	71	5.5	Very high	High	Agree
41	Bettana	-33,0796	169,151	100	6.5	Very high	Very high	Agree

ratio, AHP, and the influencing factor technique for groundwater potential mapping in a Western Ghat catchment and presented a satisfactory performance of AHP using AUC-based validation. Results of all the studies are concurrent with our findings. Therefore, the AHP-based method is the most satisfactory and popular one for assessing groundwater potential maps worldwide.

Table 9 shows verification of the correspondence between the measured borehole yield classes and the estimated groundwater potential class.

CONCLUSIONS

The subject of groundwater potential assessment has long been a concern of Basin Agencies responsible for water management and also for researchers, especially in areas with arid climates, given its importance in the supply of drinking water to its mainly rural populations. In this context, the present study has developed a rapid approach to assess the groundwater potential at the level of the arid zone of Telmzoun south of Morocco. Based on GIS data and remote sensing, in conjunction with the AHP, the developed model has integrated eight influencing variables of groundwater potentiality, including factors of geological, topographical, hydrological, and climatic origins. Its prediction performance has been evaluated using the existing borehole data coupled with the ROC curve technique. The resulting GWP map showed that there are five potentiality classes "very low", "low", "moderate", "high" and "very high". The "high" and "very high" potentiality classes cover a zone of 7.67 km2 or 37.7% of the total study area. In fact, these areas can be explored effectively by conventional methods. The AUC value of 75.5% confirms the good accuracy of the model in assessing the groundwater potential in the study area.

The developed approach can be generalized over the entire surface of the Draa and Oued Noun watershed, with little or no modifications, in order to manage and plan its resources on a large scale. This will be very useful for watershed agencies, especially in the development of master plans for the exploration, exploitation and management of groundwater resources. The resulting maps is also useful to effectively and confidently guide the drilling and exploration of groundwater resources in the study area.

Acknowledgements

We express our gratitude to all three anonymous reviewers for thoroughly assessing our work and making helpful suggestions that have substantially improved its content and reach.

REFERENCES

1. Abijith D., Saravanan S., Singh L., Jennifer J.J., Saranya T., Parthasarathy K.S.S. 2020. GIS-based multi-criteria analysis for identification of potential groundwater recharge zones - a case study from Ponnaniyaru watershed, Tamil Nadu, India. HydroResearch, 3, 1–14.
2. Adiat K.A.N., Nawawi M., Abdullah K. 2012. Assessing the accuracy of GIS-based elementary multi criteria decision analysis as a spatial prediction tool - A case of predicting potential zones of sustainable groundwater resources. J Hydrol., 440, 75–89.
3. Adiri Z., El Harti A., Jellouli A., Lhissou R., Maacha L., Azmi M., Zouhair M., Bachaoui E.M. 2017. Comparison of Landsat-8, ASTER and Sentinel 1 satellite remote sensing data in automatic lineaments extraction: A case study of Sidi Flah-Bouskour inlier, Moroccan Anti Atlas. Adv Sp Res, 60(11), 2355–2367. http://dx.doi.org/10.1016/j.asr.2017.09.006
4. Adiri Z., Harti A.E., Jellouli A., Maacha L., Bachaoui E.M. 2016. Lithological mapping using Landsat 8 OLI and Terra ASTER multispectral data in the Bas Drâa inlier, Moroccan Anti Atlas. J Appl Remote Sens.. 10(1), 016005.
5. Aggarwal M., Saravanan S., Jennifer J.J., Abijith D. 2019. Delineation of groundwater potential zones for hard rock region in Karnataka using AHP and GIS. In: Adv Sci Technol Innov. Springer Nature, 315–317.
6. Ajay Kumar V,, Mondal N,C,, Ahmed S. 2020. Identification of Groundwater Potential Zones Using RS, GIS and AHP Techniques: A Case Study in a Part of Deccan Volcanic Province (DVP), Maharashtra, India. J Indian Soc Remote Sens., 48(3), 497–511.
7. Al-Abadi A.M., Al-Temmeme A.A., Al-Ghanimy M.A. 2016. A GIS-based combining of frequency ratio and index of entropy approaches for mapping groundwater availability zones at Badra–Al Al-Gharbi–Teeb areas, Iraq. Sustain Water Resour Manag., 2(3), 265–283.
8. Al-Djazouli M.O., Elmorabiti K., Rahimi A., Amellah O., Fadil O.A.M. 2021. Delineating of groundwater potential zones based on remote sensing, GIS and analytical hierarchical process: a case of Waddai, eastern Chad. GeoJournal, 86(4), 1881–1894.
9. Al-Ruzouq R., Shanableh A., Merabtene T., Siddique M., Khalil M.A., Idris A.E., Almulla E. 2019. Potential groundwater zone mapping based on

geo-hydrological considerations and multi-criteria spatial analysis: North UAE. Catena, 173, 511–524.

10. Arumugam J. 2016. Modeling groundwater probability index in Ponnaiyar River basin of South India using analytic hierarchy process. Model earth Syst Environ., 2.
11. Arunbose S., Srinivas Y., Rajkumar S., Nair N.C., Kaliraj S. 2021. Remote sensing, GIS and AHP techniques based investigation of groundwater potential zones in the Karumeniyar river basin, Tamil Nadu, southern India. Groundw Sustain Dev., 14, 100586.
12. Benjmel K., Amraoui F., Boutaleb S., Ouchchen M., Tahiri A., Touab A. 2020. Mapping of groundwater potential zones in crystalline terrain using remote sensing, GIS techniques, and multicriteria data analysis (Case of the ighrem region, Western Anti-Atlas, Morocco). Water (Switzerland), 12(2).
13. Brauner J., Arndt M., Yajioui Z., Karaoui B., Breitkreuz C., Mahmoudi A. 2020. Cambrian shallow-marine to emergent alkaline volcanism near Ouinguigui (Ougnat inlier, eastern Anti-Atlas, Morocco): Volcanic facies, geochemistry and geodynamic setting. J African Earth Sci., 161, 103581.
14. Chen W., Li H., Hou E., Wang S., Wang G., Panahi M., Li T., Peng T., Guo C., Niu C., et al. 2018. GIS-based groundwater potential analysis using novel ensemble weights-of-evidence with logistic regression and functional tree models. Sci Total Environ., 634, 853–867.
15. Dar T., Rai N., Bhat A. 2021. Delineation of potential groundwater recharge zones using analytical hierarchy process (AHP). Geol Ecol Landscapes, 5(4), 292–307.
16. Das B., Pal S.C. 2019. Combination of GIS and fuzzy-AHP for delineating groundwater recharge potential zones in the critical Goghat-II block of West Bengal, India. HydroResearch, 2, 21–30.
17. Das N., Mukhopadhyay S. 2020. Application of multi-criteria decision making technique for the assessment of groundwater potential zones: a study on Birbhum district, West Bengal, India. Environ Dev Sustain., 22(2), 931–955.
18. Doke A.B., Zolekar R.B., Patel H., Das S. 2021. Geospatial mapping of groundwater potential zones using multi-criteria decision-making AHP approach in a hardrock basaltic terrain in India. Ecol Indic., 127, 107685.
19. Erinjery J.J., Singh M., Kent R. 2018. Mapping and assessment of vegetation types in the tropical rainforests of the Western Ghats using multispectral Sentinel-2 and SAR Sentinel-1 satellite imagery. Remote Sens Environ., 216, 345–354.
20. Ettazarini S., El Jakani M. 2020. Mapping of groundwater potentiality in fractured aquifers using remote sensing and GIS techniques: the case of Tafraoute region, Morocco. Environ Earth Sci, 79(5). https://doi.org/10.1007/s12665-020-8848-1
21. Ferozur R.M., Jahan C.S., Arefin R., Mazumder Q.H. 2019. Groundwater potentiality study in drought prone barind tract, NW Bangladesh using remote sensing and GIS. Groundw Sustain Dev., 8, 205–215.
22. El Hasnaoui A., Soulaimani A., Maacha L., Michard A., Saddiqi O., El Maidani A. 2011. Azougar n'Tilili, nouveau gîte polymétallique aurifère dans le Cambrien du Bas-Draa (Anti-Atlas occidental). Nouv Guid gé ologiques miniers du Maroc, 9, 564.
23. Ifediegwu S.I. 2022. Assessment of groundwater potential zones using GIS and AHP techniques: a case study of the Lafia district, Nasarawa State, Nigeria. Appl Water Sci, 12(1).
24. El Jazouli A., Barakat A., Khellouk R. 2019. GIS-multicriteria evaluation using AHP for landslide susceptibility mapping in Oum Er Rbia high basin (Morocco). Geoenvironmental Disasters, 6(1).
25. Jellouli A., El Harti A., Adiri Z., Chakouri M., El Hachimi J., Bachaoui E.M. 2021. Application of optical and radar satellite images for mapping tectonic lineaments in kerdous inlier of the Anti-Atlas belt, Morocco. Remote Sens Appl Soc Environ., 22, 100509.
26. Lee S., Kim Y.S., Oh H.J. 2012. Application of a weights-of-evidence method and GIS to regional groundwater productivity potential mapping. J Environ Manage., 96(1), 91–105.
27. Lentswe G.B., Molwalefhe L. 2020. Delineation of potential groundwater recharge zones using analytic hierarchy process-guided GIS in the semi-arid Motloutse watershed, eastern Botswana. J Hydrol Reg Stud., 28.
28. Machiwal D,, Jha M.K., Mal B.C. 2011. Assessment of Groundwater Potential in a Semi-Arid Region of India Using Remote Sensing, GIS and MCDM Techniques. Water Resour Manag., 25(5), 1359–1386.
29. Magesh N.S., Chandrasekar N., Soundranayagam J.P. 2012. Delineation of groundwater potential zones in Theni district, Tamil Nadu, using remote sensing, GIS and MIF techniques. Geosci Front., 3(2), 189–196.
30. Maity D.K., Mandal S. 2019. Identification of groundwater potential zones of the Kumari river basin, India: an RS & GIS based semi-quantitative approach. Environ Dev Sustain., 21(2), 1013–1034.
31. Maloof A.C., Schrag D.P., Crowley J.L., Bowring S.A. 2005. An expanded record of Early Cambrian carbon cycling from the Anti-Atlas Margin, Morocco. Can J Earth Sci., 42(12), 2195–2216.
32. Martín-Loeches M., Reyes-López J., Ramírez-Hernández J., Temiño-Vela J., Martínez-Santos P. 2018. Comparison of RS/GIS analysis with classic

mapping approaches for siting low-yield boreholes for hand pumps in crystalline terrains. An application to rural communities of the Caimbambo province, Angola. J African Earth Sci., 138, 22–31.

33. Mogaji K.A., Omobude O.B. 2017. Modeling of geoelectric parameters for assessing groundwater potentiality in a multifaceted geologic terrain, Ipinsa Southwest, Nigeria – A GIS-based GODT approach. NRIAG J Astron Geophys., 6(2), 434–451.
34. Morjani E., Abidine Z.E. 2002. Conception d'un système d'information à référence spatiale pour la gestion environnementale : application à la sélection de sites potentiels de stockage de déchets ménagers et industriels en région semi-aride (Souss, Maroc). In: [place unknown].
35. Namous M., Hssaisoune M., Pradhan B., Lee C.W., Alamri A., Elaloui A., Edahbi M., Krimissa S., Eloudi H., Ouayah M., et al. 2021. Spatial prediction of groundwater potentiality in large semi-arid and karstic mountainous region using machine learning models. Water (Switzerland), 13(16).
36. Nampak H., Pradhan B., Manap M.A. 2014. Application of GIS based data driven evidential belief function model to predict groundwater potential zonation. J Hydrol., 513, 283–300.
37. Oh H.J., Kim Y.S., Choi J.K., Park E., Lee S. 2011. GIS mapping of regional probabilistic groundwater potential in the area of Pohang City, Korea. J Hydrol., 399(3–4), 158–172.
38. Ozdemir A. 2011. GIS-based groundwater spring potential mapping in the Sultan Mountains (Konya, Turkey) using frequency ratio, weights of evidence and logistic regression methods and their comparison. J Hydrol., 411(3–4), 290–308.
39. Pande CB, Moharir KN, Panneerselvam B, Singh SK, Elbeltagi A, Pham QB, Varade AM, Rajesh J. 2021. Delineation of groundwater potential zones for sustainable development and planning using analytical hierarchy process (AHP), and MIF techniques. Appl Water Sci. 11(12).
40. Park S., Hamm S.Y., Jeon H.T., Kim J. 2017. Evaluation of logistic regression and multivariate adaptive regression spline models for groundwater potential mapping using R and GIS. Sustain., 9(7).
41. Patra S., Mishra P., Mahapatra S.C. 2018. Delineation of groundwater potential zone for sustainable development: A case study from Ganga Alluvial Plain covering Hooghly district of India using remote sensing, geographic information system and analytic hierarchy process. J Clean Prod., 172, 2485–2502.
42. Pourtaghi Z.S., Pourghasemi H.R. 2014. GIS-based groundwater spring potential assessment and mapping in the Birjand Township, southern Khorasan Province, Iran. Hydrogeol J., 22(3), 643–662.
43. Rahmati O., Nazari Samani A., Mahdavi M., Pourghasemi H.R., Zeinivand H. 2015. Groundwater potential mapping at Kurdistan region of Iran using analytic hierarchy process and GIS. Arab J Geosci., 8(9), 7059–7071.
44. Rajan Girija R., Mayappan S. 2019. Mapping of mineral resources and lithological units: a review of remote sensing techniques. Int J Image Data Fusion., 10(2), 79–106.
45. Rajasekhar M., Sudarsana Raju G., Sreenivasulu Y., Siddi Raju R. 2019. Delineation of groundwater potential zones in semi-arid region of Jilledubanderu river basin, Anantapur District, Andhra Pradesh, India using fuzzy logic, AHP and integrated fuzzy-AHP approaches. HydroResearch, 2, 97–108.
46. Razandi Y., Pourghasemi H.R., Neisani N.S., Rahmati O. 2015. Application of analytical hierarchy process, frequency ratio, and certainty factor models for groundwater potential mapping using GIS. Earth Sci Informatics, 8(4), 867–883.
47. Saaty T.L. 1980. The analytic hierarchy process McGraw-Hill. New York, 324.
48. Sajil Kumar P.J., Elango L., Schneider M. 2022. GIS and AHP Based Groundwater Potential Zones Delineation in Chennai River Basin (CRB), India. Sustainability, 14(3), 1830. https://www.mdpi.com/2071-1050/14/3/1830
49. Sapkota S., Pandey V.P., Bhattarai U., Panday S., Shrestha S.R., Maharjan S.B. 2021. Groundwater potential assessment using an integrated AHP-driven geospatial and field exploration approach applied to a hard-rock aquifer Himalayan watershed. J Hydrol Reg Stud., 37.
50. Shekhar S., Pandey A.C. 2015. Delineation of groundwater potential zone in hard rock terrain of India using remote sensing, geographical information system (GIS) and analytic hierarchy process (AHP) techniques. Geocarto Int., 30(4), 402–421.
51. Soulaimani A., Le Corre C., Farazdaq R. 1997. Déformation hercynienne et relation socle/couverture dans le domaine du Bas-Drâa (Anti-Atlas occidental, Maroc). J African Earth Sci., 24(3), 271–284.
52. Soulaimani A., Lecorre C., Bouabdelli M. 1996. Influence du socle précambrien sur la tectonique hercynienne dans l'Anti-Atlas occidental: l'exemple du poinçonnement du Bas-Drâa (Maroc). Mines, géologie et énergie, 55, 73–78.
53. Venkateswaran S., Ayyandurai R. 2015. Groundwater Potential Zoning in Upper Gadilam River Basin Tamil Nadu. Aquat Procedia, 4, 1275–1282.
54. Yao A.B., Goula B.T.A., Kane A., Mangoua O.M.J., Kouassi K.A. 2016. Cartographie du potentiel en eau souterraine du bassin versant de la Lobo (Centre-Ouest, Côte d'Ivoire) : approche par analyse multicritère. Hydrol Sci J., 61(5), 856–867.